PAPER

NaCl-template-based synthesis of TiO$_2$-Pd/Pt hollow nanospheres for H$_2$O$_2$ direct synthesis and CO oxidation†

Mareike Liebertseder,[a] Di Wang,[b] Gülperi Cavusoglu,[c] Maria Casapu, [c] Sheng Wang,[d] Silke Behrens, [d] Christian Kübel, [b] Jan-Dierk Grunwaldt [c,d] and Claus Feldmann *[a]

TiO$_2$ hollow nanosphere (HNS) are prepared *via* NaCl templates in a one-pot approach. The NaCl templates are realized by solvent/anti-solvent strategies and coated with TiO$_2$ *via* controlled hydrolysis of Ti-alkoxides. The NaCl template can be easily removed by washing with water, and the TiO$_2$ HNS are finally impregnated with Pd/Pt. Electron microscopy shows TiO$_2$ HNS with an outer diameter of 140–180 nm, an inner cavity of 80–100 nm, and a wall thickness of 30–40 nm. The TiO$_2$ HNS exhibit high surface area (up to 370 m^2 g^{-1}) and pore volume (up to 0.28 cm^3 g^{-1}) with well-distributed small Pd/Pt nanoparticles (Pt: 3–4 nm, Pd: 3–7 nm). H$_2$O$_2$ direct synthesis (room temperature, liquid phase) and CO oxidation (up to 300 °C, gas phase) are used to probe the catalytic properties and result in a good stability of the HNS structure as well as a promising performance with a H$_2$O$_2$ selectivity of 63% and a productivity of 3390 mol kg$_{Pd}$$^{-1}$ h^{-1} (TiO$_2$-Pd HNS, 5 wt%) as well as CO oxidation light-out temperatures of 150 °C (TiO$_2$-Pt HNS, 0.7 wt%).

Introduction

Nanocomposites consisting of finely dispersed noble metals (*e.g.*, Pd, Pt, Au) on high-surface-area metal oxide supports (*e.g.*, Al$_2$O$_3$, TiO$_2$, SnO$_2$, CeO$_2$) play a key-role in various fields of catalysis and gas sensing. Particularly important are, for instance, emission control,[1] electrocatalysis and fuel cells,[2] direct synthesis of H$_2$O$_2$,[3] or the detection of combustible gases.[4] The precious metal is essential to catalyze the corresponding redox reaction, and the finer its distribution on the metal oxide surface the more active surface sites are available.[1,5] In this respect, strongly interacting supports like TiO$_2$ and CeO$_2$ do not only provide a high surface area, but they also contribute to the catalytic reaction *via* perimeter sites at the noble metal-to-oxide support interface. Additionally, they allow the nanocomposite to store oxygen, which often influences the activity of the precious metal.[6]

In regard of their high relevance for heterogeneous catalysis, various composite catalysts have been suggested, including multi-component compositions and sophisticated nanostructures.[1–4,6] However, the realization of suitable nanocomposite catalysts often suffers from the fact that the nature of the active site and the specific interaction between metal oxide support and precious metal are still controversially discussed.[7] Moreover, the nanocomposite catalyst needs to be chemically and structurally stable under the transient conditions of the respective reaction (*e.g.*, in the gas phase or in the liquid phase), preferentially at elevated temperatures, as well as in the presence of moisture and reducing/oxidizing agents. In this regard, size, shape, surface area and porosity of the composite catalyst – including the metal oxide support and the deposited precious metal – play an important role. Here, new synthesis strategies and material concepts are desirable to realize composite catalysts with both high activity and high stability.

Hollow nanospheres (HNS), in principle, can provide promising features for catalysis due to their high surface area with outer surface, inner cavity and pores through the hollow sphere wall to optionally deposit precious metals.[8] Certain

[a]Institute of Inorganic Chemistry (IAC), Karlsruhe Institute of Technology (KIT), Engesserstraße 15, D-76131 Karlsruhe, Germany. E-mail: claus.feldmann@kit.edu
[b]Institute of Nanotechnology (INT), Karlsruhe Institute of Technology (KIT), Hermann-von-Helmholtz-Platz 1, 76344 Eggenstein-Leopoldshafen, Germany
[c]Institute for Chemical Technology and Polymer Chemistry (ICTP), Engesserstraße 20, 76131 Karlsruhe, Germany
[d]Institute of Catalysis Research and Technology (IKFT), Karlsruher Institute of Technology (KIT), Hermann-von-Helmholtz-Platz 1, 76344 Eggenstein-Leopoldshafen, Germany

HNS (*e.g.* CdSe) were also reported to have high mechanical and thermal stability.[9] The synthesis of HNS is typically performed *via* microemulsion techniques, Kirkendall ripening or hard-template methods.[8] Here, microemulsions suffer from low yields and sizes at the lower end of the nanoregime.[8b] Kirkendall ripening is only suitable in specific cases.[8] Hard-template methods are promising in principle provided that the template, on which the later HNS is deposited, is easy to remove and that the synthesis is easy to perform. To this respect, we here suggest a one-pot synthesis of Pd/Pt-impregnated TiO_2 HNS with a surface area of up to 370 m^2 g^{-1}, using nanosized NaCl templates. The resulting TiO_2-Pd/Pt HNS show high activity for H_2O_2 direct synthesis in the liquid phase at 30 °C as well as for CO oxidation in the gas phase up to 300 °C.

Experimental

Chemicals

TiCl(Oi-Pr)$_3$ (95%, ABCR) was handled under inert gas conditions (glove boxes or Schlenk techniques). Pt(acac)$_2$ (99.98%, Sigma Aldrich), Pd(ac)$_2$ (47.5% Pd, Acros Organics), methanol (99%, Seulberger) and NaCl (100%, VWR Chemicals) were handled as purchased. Ethanol (99.9%, Seulberger) was refluxed 3 days over Mg; THF (99%, Seulberger) was refluxed 3 days over sodium and benzophenone.

NaCl templates

A saturated solution of NaCl was prepared in methanol. Subsequently, 1 mL of this solution was injected into 20 mL of tetrahydrofuran (THF) under vigorously stirring. The resulting NaCl suspension was colloidally stable over several days.

NaCl@TiO$_2$ core–shell nanoparticles

Since the NaCl template was simultaneously dissolved upon hydrolyzing TiCl(Oi-Pr)$_3$ in a one-pot approach, a modified synthesis route had to be applied to obtain NaCl@TiO$_2$ nanoparticles for analysis. Thus, the same amount of TiCl(Oi-Pr)$_3$ was used as described below. However, only 2.5 mL of H_2O were added, which is sufficient to hydrolyze TiCl(Oi-Pr)$_3$ but not enough to also dissolve the NaCl template. Finally, the core–shell nanoparticles were washed once with EtOH and dried at 70 °C in vacuum (10^{-3} mbar).

TiO$_2$ HNS

5 mL of a 0.1 M solution of TiCl(Oi-Pr)$_3$ in ethanol were slowly added (syringe pump, 1 mL h^{-1}) to the NaCl template suspension and stirred for an additional hour. Thereafter, 5 mL H_2O were added (syringe pump, 1 mL h^{-1}). The as-prepared TiO_2 HNS were washed four times with ethanol and dried at 70 °C in vacuum (10^{-3} mbar).

TiO$_2$-Pd/Pt HNS

For impregnation of the TiO_2 HNS with Pd (5 wt%) and Pt (0.7 wt%), Pd(ac)$_2$ (5.3 mg, 0.013 mmol) and Pt(acac)$_2$ (1.2 mg,

0.005 mmol) were dissolved in acetone and added dropwise to the dried TiO_2 HNS. Thereafter, the precious metal was reduced in forming gas (H_2 : N_2 = 5 : 95) at 25 °C (Pd) and 300 °C (Pt) as indicated by the occurrence of a greyish color. Sintering of TiO_2 HNS was further studied using temperature cycles similar to those used for CO oxidation (*i.e.* 20 → 300 → 20 °C with heating/cooling rate of 5 °C min^{-1} and maintaining at 300 °C for 30 min; this cycle was performed five times).

H$_2$O$_2$ direct synthesis was performed in a semi-continuous 300 mL batch reactor (30 °C, 40 bar). The TiO_2-Pd HNS (25 mg TiO_2 with 1.3 mg Pd per experiment) were suspended in ethanol as reaction medium (200 mL). Before starting the reaction, the catalyst suspension was activated with H_2 (4 vol% in N_2, 250 mL$_{NTP}$ min^{-1}, 30 °C, 40 bar) for 1 h. Thereafter, the educt gas mixture (total flow: 250 mL$_{NTP}$ min^{-1}; gas composition: H_2/O_2/N_2 4 : 20 : 76) was introduced and stirring was started (1000 rpm). H_2, O_2 and N_2 concentrations leaving the reactor were periodically determined by micro-GC (GC: gas chromatography). N_2 was used as internal standard. The H_2O_2 concentration was analyzed *ex situ* by UV-Vis spectroscopy (ESI: Fig. S1†). H_2 conversion and H_2O_2 selectivity were determined after 63 min of reaction. Each test was repeated. The catalysts were handled in air.

CO oxidation

For the catalytic activity tests, TiO_2-Pt HNS (0.7 wt%) were used as sieved granulate fractions (125–250 μm). CO oxidation was performed in quartz microreactors (inner diameter: 1.5 mm) at atmospheric pressure at 30–400 °C (heating rate: 5 °C min^{-1}). The gas mixture (1000 ppm CO, 10% O_2 in He) was applied with a total gas flow of 50 mL min^{-1} (GHSV: 60 000 h^{-1}). Thereafter, the gas composition was detected by mass spectrometry (Pfeiffer Thermostar) at the reactor outlet (CO consumption, CO_2 formation).

Results and discussion

Materials synthesis and characterization

The realization of TiO_2-Pd/Pt HNS generally comprises the synthesis of a suitable NaCl template, the precipitation of the TiO_2 shell, and the removal of the NaCl template (Fig. 1). Whereas the advantage of the NaCl templates in view of their easy removal by washing with water is obvious, the formation of nanosized NaCl templates is more challenging at first sight. To this concern, a so-called solvent/anti-solvent strategy was used (Fig. 1; ESI: Fig. S2†). Hence, a saturated solution of NaCl in methanol was injected into tetrahydrofuran (THF). Whereas methanol is soluble in THF NaCl is not, so that the injection results in a high oversaturation of NaCl in THF. In accordance with the LaMer–Dinegar model on particle nucleation and growth,[10] this high oversaturation promotes the formation of cube-like NaCl nanoparticles, 80–100 nm in diameter (Fig. 2).

In principle, the deposition of a TiO_2 shell on the NaCl template is straightforward and can be performed in a one-pot approach (Fig. 1). In detail, however, the polarity of surfaces
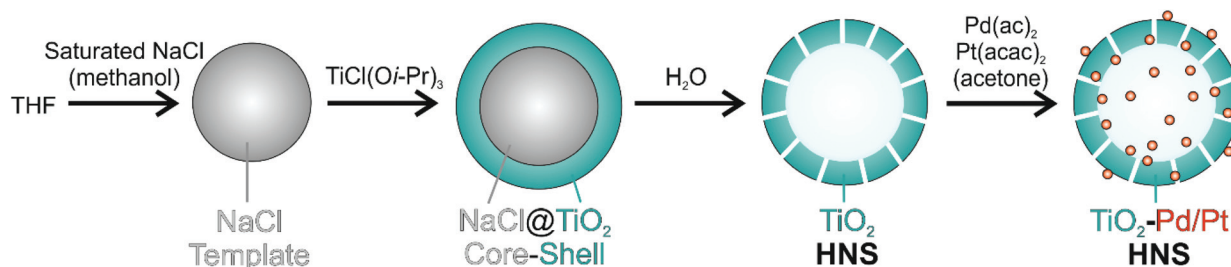
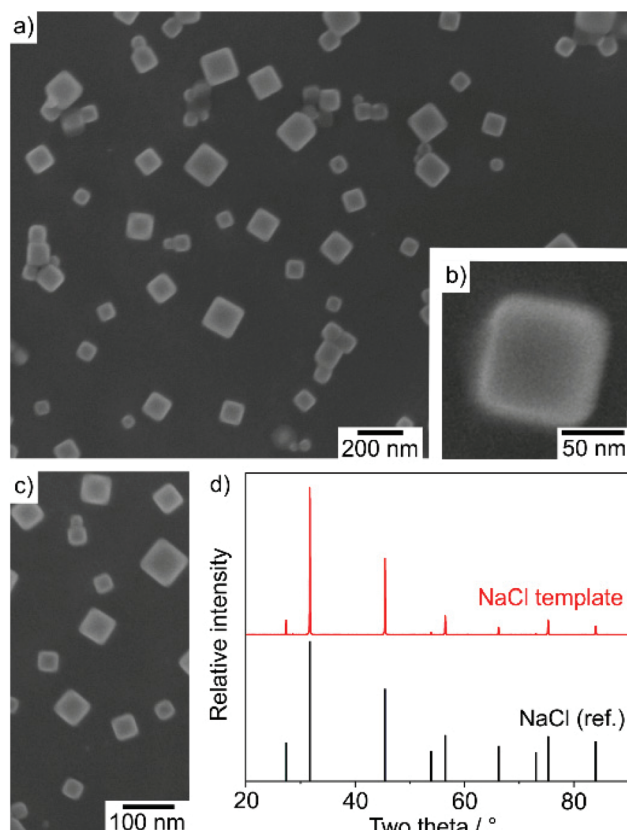**Fig. 1** Schematic one-pot synthesis of TiO$_2$-Pd/Pt hollow nanospheres (HNS) *via* NaCl templates.

Fig. 2 Cube-like NaCl templates: (a–c) electron microscopy at different levels of magnification; (d) XRD (reference: ICDD-no. 075-0306).

and the speed of the TiO$_2$ deposition become decisive. If, for instance, Ti(On-Bu)$_4$ was used and hydrolyzed upon addition of a low amount of water to the NaCl suspension in THF, we could only obtain fluffy TiO$_2$ with an incomplete coverage of the NaCl template (ESI: Fig. S3†). In a similar approach, Wang *et al.* have hydrolyzed Ti(On-Bu)$_4$ on NaCl templates in glycerol as a highly viscous liquid phase.[11] However, the resulting TiO$_2$ hollow structures were micron-sized (2–4 μm) and contain granular thin TiO$_2$ shells, which were not evaluated in regard of stability or catalytic properties. The formation of fluffy TiO$_2$ in our approach can be ascribed to the low polarity of the NaCl

surface in comparison to the highly polar surface of TiO$_2$. Consequently, the adhesion of TiO$_2$ on NaCl is low and – after formation of the very first TiO$_2$ nuclei – all additional TiO$_2$ adheres on the preformed TiO$_2$ nuclei. In an improved synthesis approach, a small portion of water was first added to pre-dissolve the NaCl surface and to increase its polarity (Fig. 1). This pre-dissolution of NaCl afterwards is indicated on TEM images by a certain gap between the NaCl template and the TiO$_2$ shell (Fig. 3). Thereafter, TiCl(Oi-Pr)$_3$ was injected, which hydrolyzes much faster than Ti(On-Bu)$_4$. As a result of both effects – the pre-hydrolyzed, more polar NaCl surface and the fast hydrolysis of the titania precursor – a uniform TiO$_2$ shell of 30–40 nm in thickness was formed on the NaCl template (Fig. 3b and c).

Finally, the NaCl template was removed from the NaCl@TiO$_2$ core–shell nanoparticles just by washing with water. The feasibility of this dissolution of course also points to the presence of pores through the TiO$_2$ sphere wall, which can be expected taking the hydrolysis and TiO$_2$ formation at room temperature into account. As a result, TiO$_2$ HNS with an outer diameter of 140–180 nm, an inner cavity of 80–100 nm, and a wall thickness of 30–40 nm were obtained (Fig. 4a and b). TEM images clearly display the cube-shaped inner cavity remaining from the former NaCl template. EDX linescans confirm the presence of the hollow-sphere structure with a characteristic dip of the Ti and O concentration profile in the center of the TiO$_2$ nanostructure (Fig. 4c and d). Moreover, the absence of Na/Cl-related signals indicates the removal of the NaCl template, which is important for catalytic studies, since especially chlorine may act as poison.

Sorption analysis evidences the porosity of the TiO$_2$ HNS and results in a high specific surface area of 370 m^2 g^{-1} and a pore volume of about 0.28 cm^3 g^{-1} (Table 1). In regard of the pore diameter, predominately micropores ($\leq$8 Å and 10–20 Å) were observed (ESI: Fig. S4 and S5†). It should also be noticed that the specific surface area of fluffy TiO$_2$ made from Ti(On-Bu)$_4$ is even higher (454 m^2 g^{-1}, Table 1). In the literature, TiO$_2$ was yet most often reported with specific surface areas <300 m^2 (g^{-1}).[12] Higher values of around 300 m^2 g^{-1} were only reported for nanorods and microspheres,[13] or TiO$_2$-SiO$_2$ composite xerogels.[14] The high porosity and surface area of the TiO$_2$ HNS are here also reflected by a significant CO$_2$ uptake (200 mg g^{-1}) and a good selectivity in comparison to N$_2$ (30 mg g^{-1}) (ESI: Fig. S6†).
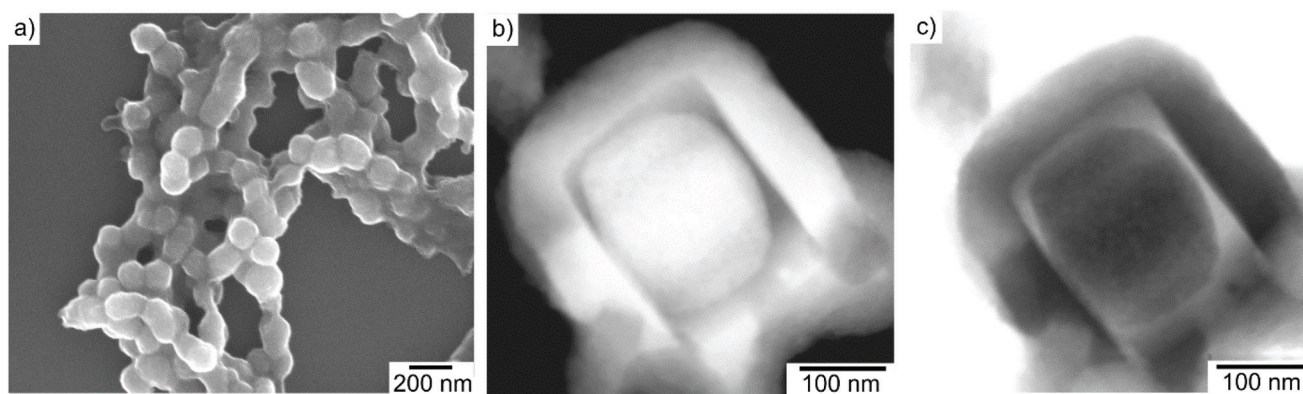
Fig. 3 NaCl@TiO$_2$ core–shell nanoparticles after hydrolysis of TiCl(Oi-Pr)$_3$: (a) electron microscopy at different levels of magnification with high-resolution bright-field (b) and dark-field (c) images (gap between NaCl core and TiO$_2$ wall observed in (b) and (c) due to pre-dissolution of NaCl).
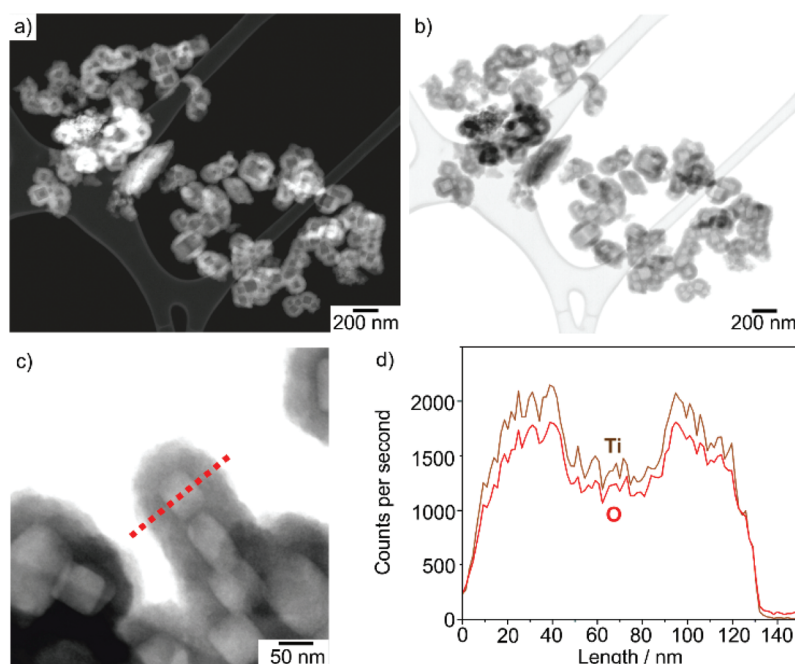

Fig. 4 TiO$_2$ HNS: (a–c) electron microscopy at different levels of magnification; (d) EDXS linescan along the dotted red line in (c).

Table 1 Specific surface area and pore volume of TiO$_2$ HNS

Material	Specific surface area/m^2 g^{-1}	Pore volume/cm^3 g^{-1}
TiO$_2$ HNS (Ti(On-Bu)$_4$, as-prepared)	454	0.236
TiO$_2$ HNS (Ti(On-Bu)$_4$, 300 °C)	19	0.015
TiO$_2$ HNS (TiCl(Oi-Pr)$_3$, as-prepared)	371	0.280
TiO$_2$ HNS (TiCl(Oi-Pr)$_3$, 300 °C)	284	0.194
TiO$_2$-Pd HNS (TiCl(Oi-Pr)$_3$, as-prepared)	226	0.189
TiO$_2$-Pt HNS (TiCl(Oi-Pr)$_3$, 300 °C)	181	0.193

Direct synthesis of H$_2$O$_2$ and CO oxidation

To evaluate the catalytic properties of the TiO$_2$ HNS, we have selected two technically relevant reactions: (i) direct synthesis of H$_2$O$_2$ from H$_2$ and O$_2$,[3] and (ii) CO oxidation.[1] These conceptually different examples allow a balanced examination at different conditions such as room-temperature catalysis in the liquid phase and catalysis at elevated temperature in the gas phase. For both test reactions, the TiO$_2$ HNS served as support and were impregnated with Pd (typically 5 wt% for H$_2$O$_2$ direct synthesis)[3] or Pt (typically 1 wt% for CO oxidation).[1,15] To this concern, solutions of Pd(ac)$_2$ and Pt(acac)$_2$ in acetone with the required concentration of precious metals were dropped on the TiO$_2$ HNS and instantaneously distributed due to capillary forces. Electron tomography shows a uniform distribution of Pd/Pt all over the TiO$_2$ HNS including outer and inner surface (Fig. 5a–c, 6a–e; ESI: Fig. S7–S13†). The Pd/Pt particle sizes are 3–4 nm (Pt) and 3–7 nm (Pd) with some larger agglomerates (about 10 nm) on the outer surface in the case of Pd.
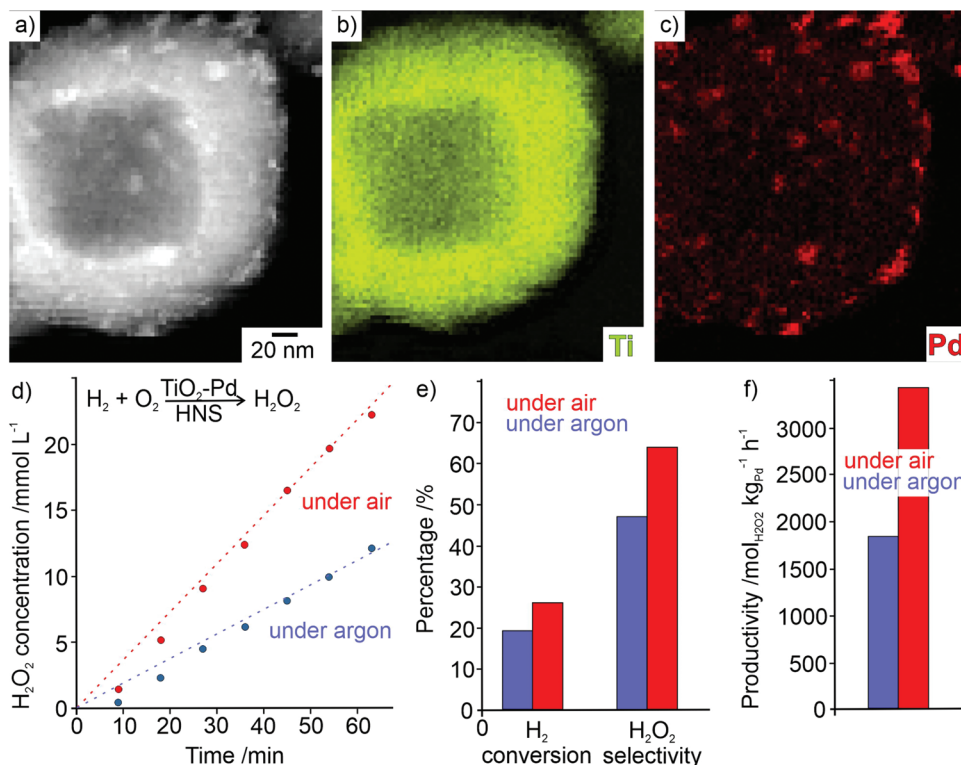
Fig. 5 TiO$_2$-Pd HNS (5 wt% Pd) for H$_2$O$_2$ direct synthesis (as-prepared): (a–c) HAADF image (a) with Ti (b) and Pd (c) element mapping; (d–f) H$_2$O$_2$ concentration over time (d), H$_2$ conversion and H$_2$O$_2$ selectivity (e), H$_2$O$_2$ productivity for catalysts stored under argon (blue) and under air (red).

H$_2$O$_2$ direct synthesis was performed with TiO$_2$-Pd HNS (5 wt% Pd) suspended in ethanol at 30 °C and 40 bar. Prior to the reaction, the catalyst suspension was treated with reducing gas (H$_2$: N$_2$ = 4 : 96). Thereafter, the reaction gas mixture (H$_2$: O$_2$: N$_2$ = 4 : 20 : 76) was introduced and stirring started (Fig. 5d–f). H$_2$, O$_2$ and N$_2$ leaving the reactor were periodically analyzed using micro-GC. The H$_2$O$_2$ concentration was analyzed *ex situ* by UV-Vis spectroscopy.[16] Accordingly, the as-prepared TiO$_2$-Pd HNS exhibit a H$_2$O$_2$ selectivity of 47% with a productivity of 1850 mol kg$_{Pd}^{-1}$ h^{-1} (Fig. 5e and f). Additionally, the TiO$_2$-Pd HNS were exposed to air resulting in an instantaneous formation of PdO as indicated by its yellow color. This oxidized form is even more active with a selectivity of 63% and a productivity of 3390 mol kg$_{Pd}^{-1}$ h^{-1} (Fig. 5e and f). These data belong to the highest values reported by now,[3a,c,16] which points to the attractiveness of the HNS material concept even for monometallic catalyst systems. According to TEM and EDXS, the HNS structure and the homogenous Pd distribution also remain subsequent to the catalytic reaction (ESI: Fig. S14†).

Contrary to the H$_2$O$_2$ direct synthesis at room temperature in the liquid phase, the CO oxidation was chosen as an example of a catalytic reaction in the gas phase at elevated temperatures. Here, sintering effects of both the TiO$_2$ HNS and the Pt nanoparticles become much more relevant and are typically observed during or after the 1st reaction cycle. CO oxi-

dation activity was tested with the TiO$_2$-Pt HNS catalyst (Fig. 6a–e, 0.7 wt% Pt, pre-treated in 5% H$_2$ at 300 °C) deposited in quartz microreactors with good heat control (∅: 1.5 mm) at 30–400 °C with a gas mixture of 1000 ppm CO and 10% O$_2$ in He at ambient pressure (Fig. 6f). The outlet gas composition was detected by mass spectrometry.

For the 1st cycle, a relatively high light-off temperature (50% of activity reached at 220 °C for the heating cycle) and a slow increase of the CO oxidation activity were observed (Fig. 6f, black arrow), which significantly changed to a sharp decrease and a light-out temperature of 153 °C (50% of activity reached for the cooling cycle, Fig. 6f, red arrow). This behavior can be ascribed to certain settling of the catalyst, including the removal of precursor traces and further crystallization of TiO$_2$ (ESI: Fig. S15–S19†). During the 2nd reaction cycle (Fig. 6f, blue/green arrow), the TiO$_2$-Pt HNS catalyst shows stable steep curves with light-off and light-out temperatures of 160 and 153 °C, respectively. These values lie within the typical conversion observed for similar catalysts and reaction parameters.[15a,17] The appearance of a typical hysteresis in the CO oxidation profile is in line with the presence of Pt particles of about 3–4 nm in size (ESI: Fig. S15, S16 and S20†) as only particles <2 nm show an inverse hysteresis.[15b] *Ex situ* X-ray absorption near edge structure (XANES) spectra collected before and after the light-off/light-out CO oxidation cycles indicate the presence of rather reduced Pt particles in the as-pre-
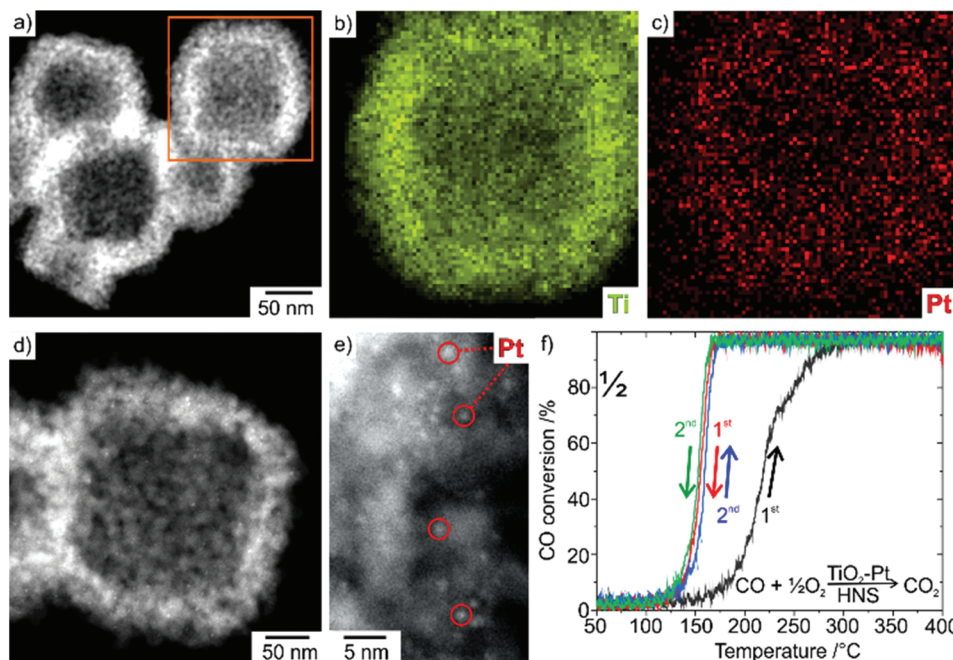
Fig. 6 TiO$_2$-Pt HNS (1 wt% Pt) for CO oxidation (pre-sintered at 300 °C, N$_2$): (a–e) HAADF image (a) with Ti (b) and Pt (c) element mapping (from orange square on (a)); (d + e) HAADF images of porous TiO$_2$ with Pt nanoparticles (indicated by red circles in (e)) at different levels of magnification; (f) temperature-dependent CO oxidation.

pared sample and slightly more oxidized particles at the end of the catalytic test (70% present as Pt(0); ESI: Fig. S21†). These XANES data align very well with the sample treatment history, since the as-prepared catalyst was reduced at 300 °C in reducing gas prior to the CO oxidation measurement. Similar to the H$_2$O$_2$ direct synthesis, the HNS-based synthesis strategy and catalyst system lead to a promising performance, which in the first shot compares to the state-of-the-art.[1]

After treatment at 300 °C, the TiO$_2$-Pt HNS (made from Ti (On-Bu)$_4$) show certain sintering as indicated by the reduction of the specific surface area from 205 to 180 m^2 g^{-1} (Table 1). Here, it also needs to be noticed that fluffy TiO$_2$ (made from Ti (On-Bu)$_4$) – originally with a very high surface area of 454 m^2 g^{-1} – shows severe sintering at 300 °C, afterwards resulting in a poor value of only 19 m^2 g^{-1} (Table 1). This finding again underlines the importance of the precursor and a controlled synthesis of the TiO$_2$ HNS. With 180–200 m^2 g^{-1} the surface area of the TiO$_2$ HNS (made from TiCl(Oi-Pr)$_3$) is still very high even after sintering. This aspect is often scarcely considered in the literature.[11–14] For CO oxidation, it is also noteworthy that the size and size distribution of the Pt nanoparticles are stable up to 300 °C with many Pt nanoparticles of 3–4 nm in size (Fig. 6a–e). A noticeable growth of the Pt nanoparticles was actually only observed above 400 °C (ESI: Fig. S20†). Based on the feasibility of synthesis and materials concept, for both catalytic applications further improvement (e.g., optimization of the concentration of the noble metal, adjustment of thermal (pre-)treatment, catalyst durability tests) will be necessary and can further improve the catalytic activity.

Conclusion

In summary, TiO$_2$ hollow nanospheres (HNS) were prepared via NaCl templates in a one-pot approach. The NaCl template was realized by solvent/anti-solvent strategies and coated with TiO$_2$ via hydrolysis of Ti-alkoxides. Precise control of the conditions of hydrolysis and TiO$_2$ formation turned out to be specifically relevant in regard of the structure and stability of the TiO$_2$ HNS. The NaCl template could be easily removed by washing with water, and the TiO$_2$ HNS were finally impregnated with Pd/Pt. Electron microscopy showed highly porous TiO$_2$ HNS (180–370 m^2 g^{-1}) with well-distributed, small Pd/Pt nanoparticles (Pd: 3–7 nm, Pt: 3–4 nm). H$_2$O$_2$ direct synthesis (liquid phase, 30 °C) and CO oxidation (gas phase, up to 300 °C) were used to probe catalysis and showed promising performance with a selectivity of 63% at a productivity of 3390 mol kg$_{Pd}^{-1}$ h^{-1} (TiO$_2$-Pd HNS, 5 wt%) and low light-off temperatures of 160 °C (TiO$_2$-Pt HNS, 0.7 wt%), respectively. Beside the synthesis strategy and the catalytic activity at very different conditions (liquid phase and room temperature as well as gas phase and temperatures up to 300 °C), especially, the stability of the TiO$_2$-Pd/Pt HNS is promising also in regard of other HNS catalysts as well as for other types of catalysis.

Conflicts of interest

The authors declare no competing financial interests.

Acknowledgements

References

1 (*a*) G. C. Dhal, S. Dey, D. Mohan and R. Prasad, *Catal. Rev.*, 2018, **60**, 437; (*b*) O. Deutschmann and J.-D. Grunwaldt, *Chem. Ing. Tech.*, 2013, **85**, 595; (*c*) R. Burch, J. P. Breen and F. C. Meunier, *Appl. Catal., B*, 2002, **39**, 283.

2 (*a*) P. Strasser, M. Gliech, S. Kuehl and T. Moeller, *Chem. Soc. Rev.*, 2018, **47**, 715; (*b*) M. Shao, Q. Chang, J. P. Dodelet and R. Chenitz, *Chem. Rev.*, 2016, **116**, 3594.

3 (*a*) S. Ranganathan and V. Sieber, *Catalysts*, 2018, **8**, 379; (*b*) R. Dittmeyer, J.-D. Grunwaldt and A. Pashkova, *Catal. Today*, 2015, **248**, 149; (*c*) J. K. Edwards, S. J. Freakley, R. J. Lewis, J. C. Pritchard and G. J. Hutchings, *Catal. Today*, 2015, **248**, 3.

4 (*a*) J. Dai, O. Ogbeide, N. Macadam, Q. Sun, W. Yu, Y. Li, B.-L. Su, T. Hasan, X. Huang and W. Huang, *Chem. Soc. Rev.*, 2020, **49**, 1756; (*b*) N. Barsan, D. Koziej and U. Weimar, *Sens. Actuators, B*, 2007, **121**, 18.

5 (*a*) Z. W. Chen, L. X. Chen, C. C. Yang and Q. Jiang, *J. Mater. Chem. A*, 2019, **7**, 3492; (*b*) C. J. Wrasman, A. Boubnov, A. R. Riscoe, A. S. Hoffman, S. R. Bare and M. Cargnello, *J. Am. Chem. Soc.*, 2018, **140**, 12930.

6 (*a*) A. M. Gänzler, M. Casapu, D. E. Doronkin, F. Maurer, P. Lott, P. Glatzel, M. Votsmeier, O. Deutschmann and J.-D. Grunwald, *J. Phys. Chem. Lett.*, 2019, **10**, 7698; (*b*) J. Jones, H. Xiong, A. T. DeLaRiva, E. J. Peterson, H. Pham, S. R. Challa, G. Qi, S. Oh, M. H. Wiebenga, X. I. Pereira Hernandez, Y. Wang and A. K. Datye, *Science*, 2016, **353**, 150; (*c*) R. Gholami, M. Alyani and K. J. Smith, *Catalysts*, 2015, **5**, 561; (*d*) M. Cargnello, T. R. Gordon and C. B. Murray, *Chem. Rev.*, 2014, **114**, 9319; (*e*) M. Cargnello, V. V. T. Doan-Nguyen, T. R. Gordon, R. E. Diaz, E. A. Stach, R. J. Gorte, P. Fornasiero and C. B. Murray, *Science*, 2013, **341**, 771.

7 (*a*) L. Liu and A. Corma, *Chem. Rev.*, 2018, **118**, 4981; (*b*) K. D. Gilroy, X. Yang, S. Xie, M. Zhao, D. Qin and Y. Xia, *Adv. Mater.*, 2018, **30**, 1706312; (*c*) N. Musselwhite and G. A. Somorjai, *Top. Catal.*, 2013, **56**, 1277.

8 (*a*) X. Wang, J. Feng, Y. Bai, Q. Zhang and Y. Yin, *Chem. Rev.*, 2016, **116**, 10983; (*b*) S. Wolf and C. Feldmann, *Angew. Chem., Int. Ed.*, 2016, **55**, 15728; (*c*) X. W. Lou, Z. Archer and Z. Yang, *Adv. Mater.*, 2008, **20**, 3987.

9 Z. W. Shan, G. Adesso, A. Cabot, M. P. Sherburne, S. A. Syed Asif, O. L. Warren, D. C. Chrzan, A. M. Minor and A. P. Alivisatos, *Nat. Mater.*, 2008, **7**, 947.

10 V. K. LaMer and R. H. Dinegar, *J. Am. Chem. Soc.*, 1950, **72**, 4847.

11 B. Wang, P. Jin, Y. Yue, S. Ji, Y. Li and H. Luo, *RSC Adv.*, 2015, **5**, 5072.

12 (*a*) Y. Ling, M. Zhang, X. Li, J. Zheng and J. Xu, *Dalton Trans.*, 2018, **47**, 10093; (*b*) X. Wang, L. Bai, H. Liu, X. Yu, Y. Yin and C. Gao, *Adv. Funct. Mater.*, 2018, **28**, 1704208; (*c*) W. Wang, D. Xu, B. Cheng, J. Yu and C. Jiang, *J. Mater. Chem. A*, 2017, **5**, 5020; (*d*) H. Liu, W. Li, D. Shen, D. Zhao and G. Wang, *J. Am. Chem. Soc.*, 2015, **137**, 13161; (*e*) D. Bu, *Appl. Surf. Sci.*, 2013, **265**, 677; (*f*) R. K. Wahi, Y. Liu, J. C. Falkner and V. L. Colvin, *J. Colloid Interface Sci.*, 2006, **302**, 530.

13 (*a*) S. Weng, X. Zhao, G. Liu, Y. Guan, F. Wu and Y. Luo, *J. Mater. Sci.*, 2018, **29**, 50; (*b*) T. V. Gerasimova, O. L. Evdokimova, A. S. Kraev, V. K. Ivanov and A. V. Agafonov, *Microporous Mesoporous Mater.*, 2016, **235**, 185; (*c*) D. Yang, M. Wang, B. Zou, G. L. Zhang and Z. Lin, *Nanoscale*, 2015, **7**, 12990.

14 (*a*) A. Mitrofanov, S. Brandes, F. Herbst, S. Rigolet, A. Bessmertnykh-Lemeune and I. Beletskaya, *J. Mater. Chem. A*, 2017, **5**, 12216; (*b*) W. Zhu, H. Yang, Y. Xie, S. Sun and X. Guo, *Mater. Res. Bull.*, 2016, **73**, 48.

15 (*a*) M. A. van Spronsen, J. W. M. Frenken and I. M. N. Groo, *Chem. Soc. Rev.*, 2017, **46**, 4347; (*b*) M. Casapu, A. Fischer, A. M. Gänzler, R. Popescu, M. Crone, D. Gerthsen, M. Türk and J.-D. Grunwaldt, *ACS Catal.*, 2017, **7**, 343.

16 S. Wang, D. E. Doronkin, M. Hähsler, X. Huang, D. Wang, J.-D. Grunwaldt and S. Behrens, *ChemSusChem*, 2020, **13**, 3243.

17 Y. Zhou, D. E. Doronkin, M. Chen, S. Wei and J.-D. Grunwaldt, *ACS Catal.*, 2016, **6**, 7799.